

CDKFormer: Contextual Deviation Knowledge-Based Transformer for Long-Tail Trajectory Prediction

Yuansheng Lian, Ke Zhang, Meng Li

Abstract—Predicting the future movements of surrounding vehicles is essential for ensuring the safe operation and efficient navigation of autonomous vehicles (AVs) in urban traffic environments. Existing vehicle trajectory prediction methods primarily focus on improving overall performance, yet they struggle to address long-tail scenarios effectively. This limitation often leads to poor predictions in rare cases, significantly increasing the risk of safety incidents. Taking Argoverse 2 motion forecasting dataset as an example, we first investigate the long-tail characteristics in trajectory samples from two perspectives, individual motion and group interaction, and deriving deviation features to distinguish abnormal from regular scenarios. On this basis, we propose CDKFormer, a Contextual Deviation Knowledge-based Transformer model for long-tail trajectory prediction. CDKFormer integrates an attention-based scene context fusion module to encode spatiotemporal interaction and road topology. An additional deviation feature fusion module is proposed to capture the dynamic deviations in the target vehicle’s status. We further introduce a dual query-based decoder, supported by a multistream decoder block, to sequentially decode heterogeneous scene deviation features and generate multimodal trajectory predictions. Extensive experiments demonstrate that CDKFormer achieves state-of-the-art performance, significantly enhancing prediction accuracy and robustness for long-tailed trajectories compared to existing methods, thus advancing the reliability of AVs in complex real-world environments.

Index Terms—trajectory prediction; long-tail learning; Transformer; contextual deviation knowledge; query-based decoding

I. INTRODUCTION

AUTONOMOUS vehicles rely on trajectory prediction to anticipate the future movements of other traffic participants [1]. This predictive ability is crucial for enabling well-informed driving decisions that prioritize both safety and traffic efficiency [2]–[4]. Current state-of-the-art (SOTA) trajectory prediction methods have demonstrated impressive performance on large-scale datasets such as Waymo Open Motion Dataset (WOMD) [5], Argoverse [6] and nuScenes [7] motion forecasting datasets. However, real-world traffic scenarios exhibit a long-tailed distribution, characterized by a multitude of rare and unusual events—such as sudden stops, erratic lane changes, or unexpected obstacles—that occur infrequently, while common and predictable scenarios, like straight driving and lane-following, dominate. This phenomenon is often referred to as the “curse of rarity” [8]. Such

an imbalance causes deep learning-based vehicle trajectory prediction models to become biased toward these frequent scenarios, struggling to accurately predict rare and atypical events that are underrepresented in the training data. Consequently, this undermines the models’ robustness and reliability, posing significant challenges for trajectory prediction models in safety-critical situations [9].

Addressing the learning of trajectory prediction models on imbalanced datasets is therefore of vital importance to enhance the reliability and safety of autonomous driving systems. Current approaches to long-tail trajectory prediction employ techniques such as data augmentation [10], [11], loss design [12], contrastive learning [13], [14], and mixture of experts [15] to improve performance on tail samples. Existing methods, however, typically overlook the explicit consideration of factors that cause long-tailed samples to be both rare and challenging to predict. A significant challenge lies in the underrepresentation of features that characterize long-tail traffic scenarios. Consequently, it becomes imperative to identify measures capable of effectively characterizing and distinguishing long-tail scenarios from common ones, and accordingly design proper methods to fuse these measures in the model.

In this study, we first conduct a comprehensive analysis of the characteristics of tailed samples and derive key metrics that quantify the target vehicle’s deviations from typical motion patterns and interactions with other agents, collectively termed deviation features. On this basis, we propose CDKFormer, a Contextual Deviation Knowledge-based Transformer model for long-tail trajectory prediction. CDKFormer is designed to learn deviation features and scene contextual features using Transformer architectures. These features are subsequently decoded using mode queries and dual future queries to generate robust trajectory predictions. We believe this will allow our model to actively focus on the abnormal parts of the traffic environment and learn more robust representations of both common and uncommon traffic conditions.

In summary, our work makes the following contributions.

- We propose a Contextual Deviation Knowledge-based Transformer (CDKFormer) for long-tail trajectory prediction. CDKFormer jointly encodes scene context and vehicle deviation status with attention mechanism, facilitating a comprehensive understanding of both regular and rare driving scenarios.
- We develop a dual query-based decoder to generate multimodal trajectory predictions. Supported by a multistream

The authors are with the Department of Civil Engineering, Tsinghua University, Beijing 100084, China (e-mail: lys22@mails.tsinghua.edu.cn; zhangkethu@mail.tsinghua.edu.cn; mengli@tsinghua.edu.cn).

Corresponding author: Meng Li.

decoder block, the decoder decodes heterogeneous scene deviation features sequentially.

- We demonstrate the effectiveness of CDKFormer through extensive experiments on benchmark datasets, showing significant improvements in predicting long-tail trajectories compared to existing SOTA methods.

The remainder of the paper is organized as follows. Section II reviews the related work. Section III defines the problem and explores the characteristics of long-tailed trajectory samples. Section IV describes the proposed model in detail. Section V presents the experimental results. Section VI concludes this work and outlines possible future directions.

II. LITERATURE REVIEW

A. Vehicle Trajectory Prediction

Vehicle trajectory prediction aims to forecast the future movements of vehicles in dynamic traffic environments. Extensive research has been dedicated to this field, leading to the development of various models that consider both vehicle dynamics and interactions among agents and map elements.

A major challenge in vehicle trajectory prediction lies in understanding agent interaction patterns. Early approaches used physics-based models [16], [17] or maneuver-based motion models [18] to estimate future trajectories. Recent advances [19]–[24] have leveraged deep learning models to address this challenge, enabling models to better capture the interaction patterns between vehicles and their surroundings, such as the road network and nearby objects, to improve prediction accuracy. Some approaches [25]–[27] further emphasize the integration of map features as vectors to enhance trajectory prediction performance. Encoding these map features in the form of polylines has proven particularly effective.

Transformers have also shown great promise in trajectory prediction tasks due to their effectiveness in processing long-range sequential data and modeling complex interactions through attention mechanisms [20], [21], [28], [29]. For instance, QCNet [21] leverages attention mechanisms to model interactions at different spatial and temporal scales, enabling more accurate and robust predictions in real-time traffic scenarios. Furthermore, some studies explore variations in Transformer architectures [30] or attention mechanism [31] to better fuse spatio-temporal contextual information.

B. Query-Based Trajectory Decoding

Most recent end-to-end trajectory prediction models adopt a query-based trajectory decoding paradigm, inspired by Detection Transformer (DETR) [32] from the object detection field. Query refers to a set of learnable embedding vectors that serve as placeholders for future trajectory predictions. These queries interact with encoded scene features through attention mechanisms within the Transformer architecture, enabling the model to generate distinct and contextually relevant trajectory forecasts. Various terms have been used to describe this underlying concept, such as “proposals” in mmTransformer [28], “anchor trajectories” in MultiPath++, “queries” in MTR [20], SEPT [33], and QCNet [21], etc.

Various studies have contributed to improvements in query design. Early studies utilize predefined queries to inform the model of possible endpoints [20], [34], [35]. Recent studies purpose to decode trajectories dynamically with learnable queries [21], [36]. The queries are designed to capture the learned contextual information with cross-attention mechanism and produce multi-modal future trajectories. A recent study [2] proposes endpoint-risk-combined intention queries as prediction priors to support risk-aware risk prediction.

C. Long-Tail Trajectory Prediction

Long-tail learning addresses the challenge of imbalanced data distributions, where a large portion of the dataset consists of rare or less frequent examples. In the trajectory prediction field, various strategies have been proposed to tackle this issue, including data augmentation [10], [11], loss design [12], contrastive learning [13], [14], mixture of experts [15], model ensemble [37], etc.

Input data augmentation techniques are utilized to improve the accuracy and robustness of trajectory prediction, incorporating strategies such as heading rotation, scene flipping, and adding random noise. These strategies have been shown to increase robustness against adversarial patterns in trajectories [10], [38]. The design of synthetic driving data has also demonstrated notable benefits for trajectory prediction [11].

Contrastive learning (CL) was first proposed to deal with long-tail issue in trajectory prediction by [13]. They propose to improve long-tail trajectory prediction performance by forcing similar samples together and pulling dissimilar samples apart in the feature space by a contrastive loss function. [14] propose FEND, a feature-enhanced distribution aware CL framework that utilize prototypical contrastive learning (PCL). A following study [39] further integrates contextual scene information in the contrastive learning framework. However, the scene contextual interaction information is not explicitly considered in their contrastive learning framework. Researchers [40] also extends the use of contrastive learning by considering subclasses dynamically. [41] propose a hierarchical wave-semantic contrastive learning (Hi-SCL) framework, which maintains a collection of feature-enhanced hierarchical prototypes, dynamically steering trajectory samples closer or pushing them farther away.

Contrastive learning typically functions by differentiating between positive and negative sample pairs. In current contrastive learning-based trajectory prediction methods, the contrastive sample pairs are often constructed based on either the difficulty scores [13] or the clustering of focal agent motion patterns [14], frequently overlooking information from interacting agents and the dynamic environment. This approach poses significant challenge in effectively constructing positive and negative sample pairs that incorporate scene semantics [42], which in turn hinders the development of a robust contrastive loss function. In this paper, we avoid the challenge of attempting to apply contrastive learning to consistently consider both interacting- and scene-level clustering. Alternatively, we approach the long-tail trajectory prediction through deviation knowledge fusion and dual query-based decoding

with loss reweighting. We posit that both the individual motion and interaction patterns contribute to the rarity of traffic scenarios and should be carefully designed and incorporated into the model design.

III. LONG-TAIL CHARACTERISTICS OF TRAJECTORY DATA

A. Preliminaries

Given a series of d_a -dimensional observed motion features $\mathbf{X} \in \mathbb{R}^{N_a \times T_o \times d_a}$ for N_a agents, including the target vehicle and its surrounding agents, over a time span T_o and high-definition (HD) map vectors $\mathbf{I} \in \mathbb{R}^{N_m \times l_m \times d_m}$ of N_m map polylines, our objective is to predict future positions $\mathbf{Y} \in \mathbb{R}^{T_f \times 2}$ of the target vehicle in a certain time horizon T_f . Specifically, we seek to train a neural network to model the mapping $f(\mathbf{Y}|\mathbf{X}, \mathbf{I})$. Additionally, we introduce a long-tail score S to quantify the likelihood of a sample belonging to the tail of the data distribution. On this basis, we seek to enhance the model's predictive performance in these long-tail scenarios while not affecting the overall performance.

B. Long-Tail Definition

Long-tail learning aims to train a deep neural network on a dataset with a long-tailed class distribution, where a small proportion of classes contain a large number of samples, while the majority of classes are represented by only a few samples [43]. In classification tasks, it is relatively straightforward to identify tail samples. However, long-tail trajectory prediction is essentially a long-tail regression task [44], where the labels (future trajectories) are continuous values. In this case, hard classification boundaries among classes do not exist [43]. Previous studies identify tailed samples by a difficulty score, which is computed by the (final) displacement error performance of a Kalman filter [13], [45] or a trained prediction network [14].

In this study, we propose measuring a tailed sample with both its difficulty and rarity. We believe that tailed trajectories are not only samples that are challenging to predict, but also tend to exhibit more complex motion patterns and diverse interaction types, making them relatively rare in spatio-temporal distribution. While these two aspects are not identical, they are closely related and should be considered together in a holistic manner. Similar to [14], we quantify the difficulty score S_d as the average displacement error of the predictions of a trained model. The rarity score S_r is determined by the negative log-likelihood of a Gaussian Mixture Model (GMM). As illustrated in Fig. 1, the GMM models the distribution of trajectory final points. Samples that are less likely to occur within the learned distribution (i.e., those farther from the Gaussian components) are assigned higher rarity scores. Finally, the tail score S is computed as the square root product of difficulty and rarity:

$$S = \sqrt{S_d \times S_r} \quad (1)$$

The tail score distribution of training samples in Argoverse 2 motion forecasting dataset is demonstrated in Fig. 2.

C. Long-Tail Characteristics

A pivotal and often underexplored question in current research persists: What inherent characteristics can represent long-tailed trajectory samples? Furthermore, which metrics are most effective in elucidating the attributes of these trajectories and the surrounding traffic scenarios? In this section, we present a comprehensive analysis of the distinct features that differentiate long-tailed trajectory samples from head samples.

Utilizing Argoverse 2 motion forecasting dataset [6], we investigate the long-tail characteristics of the target vehicle trajectories from two perspectives: individual motion and group interaction. Our analysis focuses on comparing the top 10% of tailed samples with the top 10% of head samples, based on the defined tail score. The following metrics are proposed to quantitatively measure the deviations in individual motion and group interactions between tailed and normal scenarios.

- Individual Deviation

- ΔV_{ind} : change in target vehicle's velocity in the observation window, in m/s
- ΔH_{ind} : change in target vehicle's heading in the observation window, in degrees
- $\sigma(V_{\text{ind}})$: standard deviation of target vehicle's velocity in the observation window, in m/s
- $\sigma(H_{\text{ind}})$: standard deviation of target vehicle's heading in the observation window, in degrees

- Group Deviation

- ΔV_{grp} : average relative speed between target vehicle and other surrounding traffic agents at the end of observation window, in m/s
- $\sigma(H_{\text{grp}})$: standard deviation of target vehicle and other surrounding traffic agents' headings at the end of observation window, in degrees

These metrics, which represent the complexity of traffic scenarios surrounding the target vehicle, are independent of vehicle absolute positions. Consequently, they can be utilized to effectively assess the deviation of the current traffic state in a coordinate-agnostic way.

A descriptive table on these metrics and the results of significance comparisons from ANOVA tests are summarized in Table I. The distributions of individual and group deviation measures are shown in Fig. 3 and Fig. 4, respectively. As a result, tail samples exhibit significantly higher mean changes in velocity and greater variability in both velocity and heading. For example, among the top 10% of tail samples, 26.74% involve clear turning maneuvers, while the remaining 73.26% proceed straight. In contrast, 88.28% of the top 10% head samples follow straight trajectories. Additionally, tail samples show more dynamic agent interactions with higher relative speed and greater group heading variability. These distinctions underscore the complexity and unpredictability inherent in long-tailed vehicle trajectories, highlighting the necessity of incorporating these features to fully understand and model long-tail traffic scenarios.

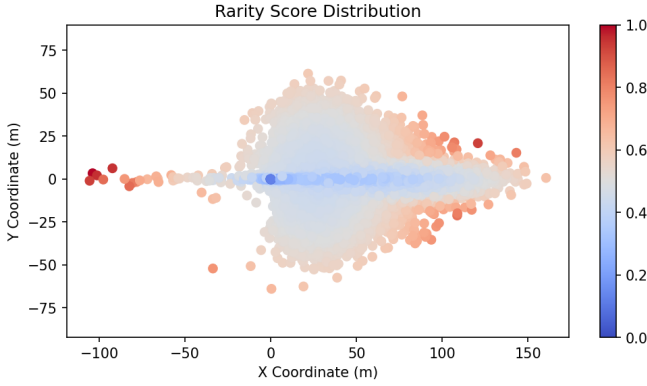


Fig. 1. Rarity score distribution of the training samples in Argoverse 2 motion forecasting dataset. The normalized trajectory endpoints are fitted to a GMM with 6 components. For each trajectory sample, the rarity score is calculated as the negative log-likelihood of its endpoint under the learned distribution. These scores are then normalized to the range [0, 1], with higher scores indicating higher rarity.

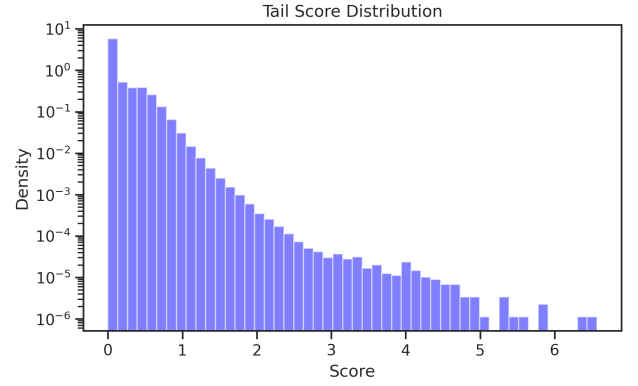


Fig. 2. Tail score distribution of the training samples in Argoverse 2 motion forecasting dataset. Tail score is calculated as the production of difficulty score and rarity score. Tail score is shown in log-scale.

TABLE I
LONG-TAIL CHARACTERISTICS OF TRAJECTORY SAMPLES IN ARGOVERSE 2 MOTION FORECASTING DATASET.

| Category | Metric | Tail | Head | p-value |
|------------|-------------------|-------------------|-------------------|---------|
| Individual | ΔV_{ind} | 1.37 ± 3.59 | -0.14 ± 0.75 | <.001 |
| | ΔH_{ind} | 0.12 ± 77.07 | -0.12 ± 18.06 | .69 |
| | $\sigma(V_{ind})$ | 1.10 ± 0.85 | 0.05 ± 0.26 | <.001 |
| Group | $\sigma(H_{ind})$ | 13.09 ± 33.49 | 0.59 ± 8.24 | <.001 |
| | ΔV_{grp} | 5.59 ± 3.46 | 0.79 ± 1.20 | <.001 |
| | $\sigma(H_{grp})$ | 76.58 ± 42.91 | 42.00 ± 47.93 | <.001 |

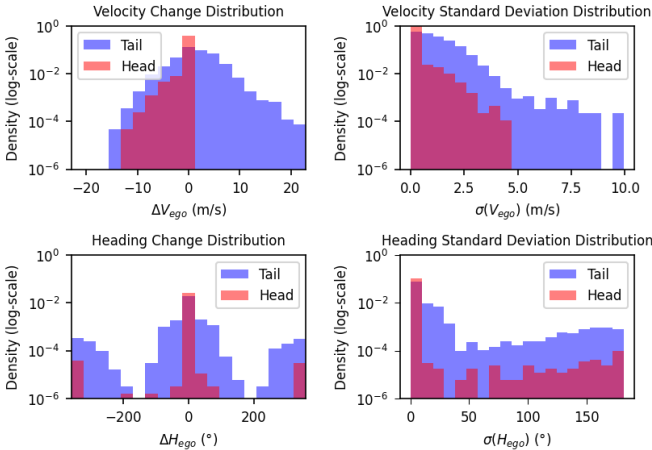


Fig. 3. Distribution of speed difference, speed standard deviation, heading difference and heading standard deviation of top 10% head and tail samples. The y-axis (density) is in log scale.

IV. METHODOLOGY

A. Prediction Framework Overview

The proposed CDKFormer framework is illustrated in Fig. 5. CDKFormer is constructed in an encoder-decoder way. In the scene encoder, we first encode the HD map vectors and agent motion information and fuse them in a scene context fusion module. The deviation feature is learned in parallel with a

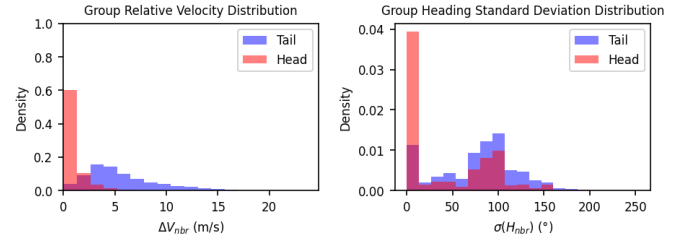


Fig. 4. Distribution of relative speed and heading of top 10% head and top 10% tail samples.

deviation fusion module. Then, the learned context feature and deviation feature are jointly decoded in a query-based paradigm. A mode query and dual future queries are initiated to interactively and progressively extract the context and deviation feature through multistream decoder blocks. Then a scene query is obtained by a learnable gating mechanism. We additionally refine this scene query and generate the final multimodal trajectory predictions.

B. Scene Context Encoding

1) *Agent Motion Encoding*: The agent motion input of the module is a 6-dimensional vector $\mathbf{X} \in \mathbb{R}^{N_a \times T_o \times d_a}$, where $d_a = 6$ includes the 2D historical position, positional displacement vector, positional displacement magnitude, and absolute velocity. Fourier embedding [46] is first applied to these motion inputs, followed by a multilayer perceptron (MLP) to project them into a high-dimensional space, producing the group motion encoding $\mathbf{X}_a \in \mathbb{R}^{N_a \times T_o \times d}$. Then, we apply a standard Transformer encoder on \mathbf{X}_a , which is composed of a multihead attention and an MLP, with layer normalization and residual connections added. This enables feature aggregation in the temporal dimension. The multihead

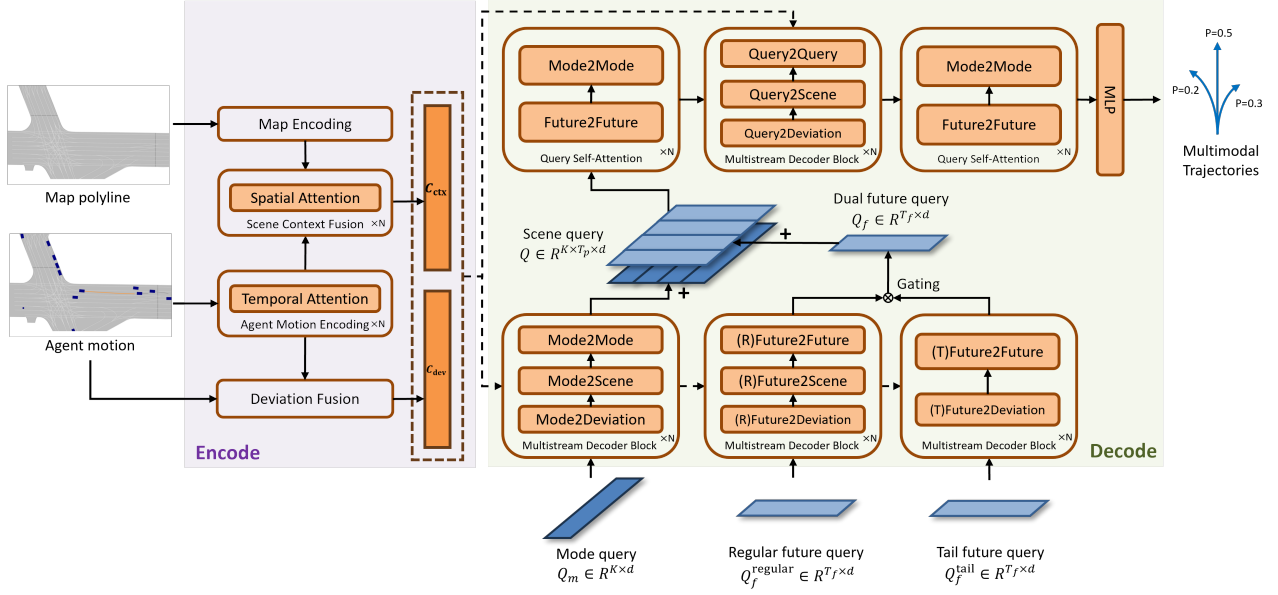


Fig. 5. Overview of the proposed CDKFormer architecture. The model first encode the agent motion and scene contextual information with self-attention-based encoders. The deviation and motion features of the target vehicle are jointly fused in a deviation fusion module. The scene context and deviation information are subsequently decoded by a mode query and dual future queries, including a regular future query and a tail future query, within multistream decoder blocks. Then, a scene query is obtained by combining the mode query and weighted combined future query. This scene query is further refined and used for multimodal trajectories generation. $\times N$ denotes N stacked layers. (R)Future and (T)Future denote regular future query and tail future query, respectively.

attention is calculated as follows.

$$\text{MultiHeadAttention}(Q, K, V) = \text{softmax}\left(\frac{QK^T}{\sqrt{d_k}}\right)V \quad (2)$$

$$Q = XW^Q \quad (3)$$

$$K = XW^K \quad (4)$$

$$V = XW^V \quad (5)$$

where W^Q , W^K and W^V are weight matrix, X is the input, d_k is the hidden state dimension. The encoder layer is repeated for N times to obtain the motion feature $\tilde{X}_a \in \mathbb{R}^{N_a \times T_o \times d}$, which represents the motion dynamic of both the target vehicle and its surrounding agents. Then we extract the target vehicle's motion feature $X_{\text{tgt}} \in \mathbb{R}^{T_o \times d}$ from \tilde{X}_a , which will be used for deviation feature fusion in Section IV-C. The final agent motion encoding is obtained by extracting the last timestep of \tilde{X}_a , denoted as $C_a \in \mathbb{R}^{N_a \times d}$.

2) *Map Encoding*: The input HD map feature $I \in \mathbb{R}^{N_m \times l_m \times d_m}$ comprises positions and displacement vectors of centerlines surrounding the target vehicle, organized into N_m polylines, each containing l_m points with $d_m = 4$. We encode these polylines with a PointNet-like encoder [47], as also employed in [20], [48].

The polyline encoder first applies an MLP to project each polyline into the high-dimensional space, producing local features $I_l \in \mathbb{R}^{N_m \times l_m \times d}$. Max-pooling is then performed along the local polyline dimension to obtain global feature $I_g \in \mathbb{R}^{N_m \times d}$. By combining the local feature I_l and the global feature I_g through addition, we update the polyline representations. Then, this MLP and max-pooling process is applied iteratively to derive the map encoding $C_m \in \mathbb{R}^{N_m \times d}$.

3) *Scene Context Fusion*: Scene context fusion is conducted to fully integrate traffic agent motion and map infor-

mation, enabling a semantic understanding of dynamic traffic environments. We first concatenate $C_a \in \mathbb{R}^{N_a \times d}$ and $C_m \in \mathbb{R}^{N_m \times d}$ to a scene encoding $C_{\text{sce}} \in \mathbb{R}^{(N_a+N_m) \times d}$. The spatial embeddings are generated by mapping the central positions of N_a agents and N_m lane vectors into a d -dimensional space, which are then added to C_{sce} . Then, this scene encoding is fed into another standard Transformer encoder to enhance agent-lane spatial interaction, producing the scene context feature $C_{\text{ctx}} \in \mathbb{R}^{(N_a+N_m) \times d}$.

C. Deviation Feature Fusion

As discussed in Section III-C, features that describe deviations in the current vehicle state from the normal state can serve as indicators of long-tailed scenarios. Therefore, in the encoding process, we specifically model these deviation features from both the target vehicle and agent interaction perspectives, providing a comprehensive understanding of the deviation state of the surrounding traffic environment.

We introduce deviation inputs including both target vehicle and agent interaction perspectives, as shown in Fig. 6. The individual deviation input $X_{\text{dev}}^{\text{ind}} \in \mathbb{R}^{T_o \times 6}$ comprises several components. As illustrated in Fig. 7, let θ^t and v^t represent the absolute heading angle and velocity of the target vehicle at time t , respectively. Additionally, let α^t denote the orientation of the vehicle's displacement vector at time t . We employ a 6D descriptor to encapsulate the individual deviation feature $X_{\text{dev}}^{\text{ind}}$, defined as $[\theta^t - \theta^0, \theta^t - \alpha^0, \theta^t - \alpha^t, \sqrt{\frac{1}{t} \sum_t (\theta^t - \bar{\theta})^2}, v^t - v^0, \sqrt{\frac{1}{t} \sum_t (v^t - \bar{v})^2}]$. This descriptor comprises six components: the change in heading, the change in heading relative to the initial displacement orientation, the angle between heading and the current displacement orientation, the standard

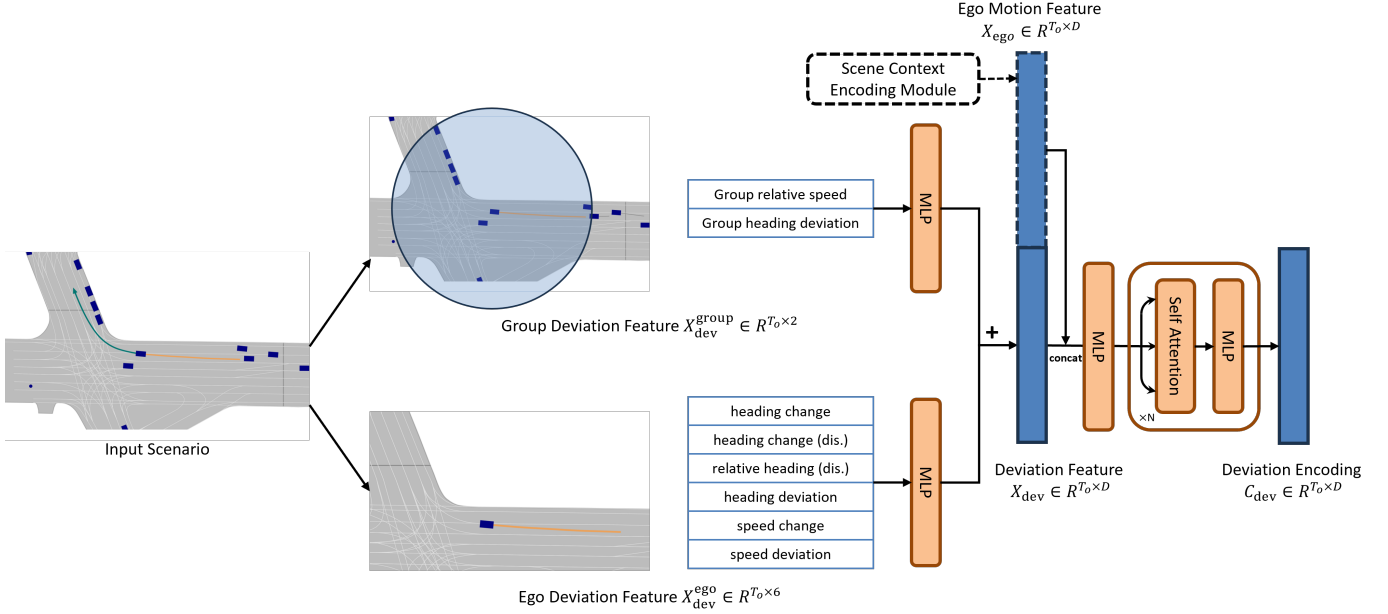


Fig. 6. Deviation feature encoding module structure. The individual and group deviation feature are first separately encoded with MLPs and then added to form a unified deviation feature. Then this deviation feature is fused with the target motion feature using a Transformer encoder, which facilitates the modeling of temporal deviation patterns.

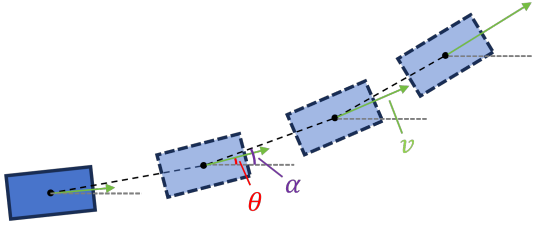


Fig. 7. Illustration of target vehicle heading angle and speed.

deviation of heading, the change in velocity, and the standard deviation of velocity. These metrics can be used to quantify directional changes and variability in motion and velocity, and are irrelevant to current positions or coordinates. The group deviation feature X_{dev}^{grp} can be formulated as a 2D vector: $[\frac{1}{N_a} \sum_{n=1}^{N_a} (v_n^t - v^t), \sqrt{\frac{1}{N_a} \sum_{n=1}^{N_a} (\theta_n^t - \bar{\theta}^t)^2}]$, including the surrounding agents' velocity relative to the target vehicle and group heading deviation.

Both the individual and group deviation features are separately projected into high-dimensional spaces using MLPs. The resulting representations are then added to form a comprehensive deviation feature $X_{dev} \in \mathbb{R}^{T_o \times d}$. Subsequently, deviation fusion is performed by concatenating X_{dev} and X_{tgt} , followed by an MLP-based fuser and a Transformer encoder layer to capture temporal dependencies. The final output deviation feature C_{dev} is passed to the decoder along with C_{ctx} , providing insights into both scene contextual information and motion deviation status.

D. Dual Query-Based Trajectory Decoding

With the advancement of query-based decoding techniques in trajectory prediction tasks, researchers have extensively

explored the use of distinct queries to dynamically decode future trajectories [20], [21], [36]. In this paper, we propose to decode future trajectories using a mode query and dual future queries. The mode query $Q_m \in \mathbb{R}^{K \times d}$ captures the diversity of different modes, supporting multimodal prediction. The dual future queries consist of a regular future query $Q_f^{regular} \in \mathbb{R}^{T_f \times d}$ and a tail future query $Q_f^{tail} \in \mathbb{R}^{T_f \times d}$. $Q_f^{regular}$ is designed to model the future dynamics of the target vehicle, while Q_f^{tail} is intended to capture the deviation status of the current traffic scenario, thereby reflecting the long-tail characteristics of a trajectory sample. These queries are initialized in the decoder and then processed through multistream decoder blocks, allowing the model to simultaneously integrate both scene-level contextual information and vehicle deviation status.

1) *Multistream Decoder Block*: We facilitate the simultaneous learning of contextual and deviation information through a multistream decoder block. The multistream decoder block is a crucial module in our model, designed to process and integrate multiple streams of information using attention mechanisms. In a single multistream decoder block, multiple distinct information streams are processed independently yet simultaneously, allowing for continuous processing within the same block.

The computational flow of our multistream decoder block is formally described in Algorithm 1. The input of a multistream decoder block is one query and a stream of memory features, which can be heterogeneous in shape and type. In the first cross-modal fusion phase, each feature stream undergoes layer normalization before being processed through a multihead

Algorithm 1 Pseudo Code of MultiStream Decoder Block Forward Pass

Input: Query Embedding Q , Heterogeneous Feature Streams $S = \{S_i\}_{i=1}^{n_s}$

Output: Refined Query \hat{Q}

```

1: for each feature stream  $S_i \in S$  do
2:    $Q_{\text{attn}} \leftarrow \text{MultiHeadAttention}(\text{LayerNorm}(Q), \text{LayerNorm}(S_i), \text{LayerNorm}(S_i))$ 
3:    $Q \leftarrow Q + \text{Dropout}(Q_{\text{attn}})$ 
4:    $Q_{\text{mlp}} \leftarrow \text{MoE}(Q, \{\text{Expert}_k\}_{k=1}^K)$ 
5:    $Q \leftarrow Q + \text{Dropout}(Q_{\text{mlp}})$ 
6: end for
7:  $Q_{\text{attn}} \leftarrow \text{MultiHeadAttention}(\text{LayerNorm}(Q), \text{LayerNorm}(Q), \text{LayerNorm}(Q))$ 
8:  $Q \leftarrow Q + \text{Dropout}(Q_{\text{attn}})$ 
9:  $Q_{\text{mlp}} \leftarrow \text{MLP}(\text{LayerNorm}(Q))$ 
10:  $\hat{Q} \leftarrow Q + \text{Dropout}(Q_{\text{mlp}})$ 
11: return  $\hat{Q}$ 

```

attention mechanism:

$$Q_{\text{attn}} = \text{MultiHeadAttention}(\text{LayerNorm}(Q), \quad (6)$$

$$\text{LayerNorm}(S_i), \quad (7)$$

$$\text{LayerNorm}(S_i)) \quad (8)$$

where S_i represents the i -th input feature stream. The attention outputs are integrated into the query representation through residual dropout connections. Subsequent to attention-based fusion, a Mixture-of-Experts (MoE) layer enhances feature representation:

$$Q_{\text{mlp}} = \sum_{k=1}^K G_k(Q) \cdot \text{Expert}_k(Q) \quad (9)$$

where G_k denotes learned gating weights of the k -th expert. Each expert is essentially an MLP, enabling conditional computation based on input characteristics. The final fusion stage employs self-attention over the aggregated representation, followed by another MLP layer to project features into the target space.

$$Q_{\text{final}} = \text{MultiHeadAttention}(\text{LayerNorm}(Q), \quad (10)$$

$$\text{LayerNorm}(Q), \quad (11)$$

$$\text{LayerNorm}(Q)) \quad (12)$$

Our multistream decoder block design allows the model to capture complex interactions and long-range dependencies between the memory features and the query. The combination of cross-attention, MoE MLP layers, and self-attention empowers the model to effectively aggregate and leverage diverse information sources, capturing both intermodal and intramodal relationships. The final multistream decoder is the stack of multistream decoder blocks.

2) *Dual Query-Based Trajectory Decoder*: We propose decoding future trajectories in CDKFormer utilizing the multistream decoder block introduced in Section IV-D1. The multistream decoder block is structured distinctly for each

query type to accommodate both fine-grained scene understanding and long-tail trajectory prediction. For the mode query and the regular future query, the multistream decoder block operates through two distinct streams: the deviation feature $C_{\text{dev}} \in \mathbb{R}^{T \times d}$, which learns the motion and deviation patterns of the target vehicle, and the contextual encoding $C_{\text{ctx}} \in \mathbb{R}^{(N_a + N_m) \times d}$, which sequentially captures scene semantics. This multistream fusion paradigm supports spatial-temporal knowledge learning. For the tail future query, the multistream decoder block processes only the deviation feature stream, aiming to primarily extract the motion and deviation status of the target vehicle. The dual future query design allows two queries to each carry out the task of learning regular and irregular traffic state dynamic, potentially enhancing long-tail trajectory prediction. The calculation is shown below.

$$Q_m = \text{MultiStreamDecoder}(Q_m, (C_{\text{dev}}, C_{\text{ctx}})) \quad (13)$$

$$Q_f^{\text{regular}} = \text{MultiStreamDecoder}(Q_f^{\text{regular}}, (C_{\text{dev}}, C_{\text{ctx}})) \quad (14)$$

$$Q_f^{\text{tail}} = \text{MultiStreamDecoder}(Q_f^{\text{tail}}, C_{\text{dev}}) \quad (15)$$

Then, we combine the dual queries through a learnable gating mechanism. The gate weights are learned through an MLP-based router module. The input of the router module is the concatenated dual queries. The tail weight $\gamma \in \mathbb{R}^{T_f \times d}$ is generated and subsequently used for dual query combination as follows.

$$Q_f^{\text{dual}} = \gamma Q_f^{\text{tail}} + (1 - \gamma) Q_f^{\text{regular}} \quad (16)$$

Then, we add Q_m and Q_f^{dual} to get a scene query $Q \in \mathbb{R}^{K \times T_f \times d}$.

$$Q = Q_m[:, \text{None}, :] + Q_f^{\text{dual}}[\text{None}, :, :] \quad (17)$$

To allow the scene query to fully learn the temporal dependency among difference modalities, we apply self-attention block on time and modality dimension subsequently. The scene query is converted to a dense feature in shape $\mathbb{R}^{K T_f \times d}$ before the refinement, similar to [36]. Then, we update the scene query Q with another multistream decoder block.

$$Q = \text{MultiStreamDecoder}(Q, (C_{\text{dev}}, C_{\text{ctx}})) \quad (18)$$

Afterwards, another self-attention based refinement is conducted, followed by an MLP to generate future multimodal trajectories and the corresponding probability scores.

E. Learning Objectives

In this study, we employ distinct loss functions to regulate the learning of different query types. Specifically, a smoothed L1 regression loss is applied to the predictions of mode queries, future queries, and scene queries. For mode learning in both mode and scene queries, we utilize a cross-entropy classification loss. The winner-takes-all strategy is adopted. Additionally, we apply a regression loss on the predicted future

positions of neighboring agents learned from the contextual feature.

$$\mathcal{L}_{\text{mode}} = \mathcal{L}_{\text{mode}}^{\text{reg}} + \mathcal{L}_{\text{mode}}^{\text{cls}} \quad (19)$$

$$\mathcal{L}_{\text{future}} = \mathcal{L}_{\text{future}}^{\text{reg}} \quad (20)$$

$$\mathcal{L}_{\text{scene}} = \mathcal{L}_{\text{scene}}^{\text{reg}} + \mathcal{L}_{\text{scene}}^{\text{cls}} \quad (21)$$

$$\mathcal{L}_{\text{grp}} = \mathcal{L}_{\text{grp}}^{\text{reg}} \quad (22)$$

$$\mathcal{L}_*^{\text{reg}} = \begin{cases} \frac{1}{t_f} \sum_t^{t+t_f} \frac{1}{2} (\hat{y}^t - y^t)^2, & \text{if } |\hat{y}^t - y^t| < 1 \\ \frac{1}{t_f} \sum_t^{t+t_f} (|\hat{y}^t - y^t| - 0.5), & \text{o.w.} \end{cases} \quad (23)$$

$$\mathcal{L}_*^{\text{cls}} = - \sum_{k=1}^K p_k \log(\hat{p}_k) \quad (24)$$

where \hat{y}^t and y^t is the predicted and ground-truth future position at time t , and p_k is the probability for selecting mode k as the best mode. \hat{p}_k is the ground-truth best prediction index.

The tail query Q_t is designed especially to generate accurate future 2D position on tailed samples. Following the idea of label distribution smoothing (LDS) in [44], we introduce a tail loss weighted by smoothed tail score S .

$$\mathcal{L}_{\text{tail}} = \tilde{S} \cdot \mathcal{L}_{\text{tail}}^{\text{reg}} \quad (25)$$

where \tilde{S} is the tail score smoothed with a Gaussian kernel. $\mathcal{L}_{\text{tail}}^{\text{reg}}$ is the regression loss on tail query predictions. The hard samples are therefore given higher weights to support imbalanced regression. The final loss function is calculated as follows.

$$\mathcal{L} = \mathcal{L}_{\text{mode}} + \mathcal{L}_{\text{future}} + \mathcal{L}_{\text{scene}} + \mathcal{L}_{\text{grp}} + \alpha \mathcal{L}_{\text{tail}} \quad (26)$$

where α is the tail loss weight.

V. EXPERIMENTS

A. Experimental Settings

1) *Dataset*: We use Argoverse 2 motion forecasting dataset [6] to validate the performance of CDKFormer. The Argoverse 2 motion forecasting dataset consists of 250,000 scenarios for training and validation. Each scenario lasts 11 seconds and includes the 2D bird’s-eye view of the centroid and heading of each tracked object, sampled at 10 Hz.

2) *Baseline Comparison*: We compare our model with the following SOTA trajectory prediction models: VectorNet [26], LaneGCN [25], MTR [20] and QCNet [21].

We also implement two SOTA long-tail trajectory prediction methods as comparison baselines to verify the long-tail performance of the proposed model: Contrastive [13] and FEND [14]. Additionally, we compare two naive long-tail learning approaches: data balanced sampling and loss reweighting. The sampling and reweighting factors are set as the tail scores of each sample. Long-tail learning methods are implemented using QCNet as the backbone.

TABLE II
PREDICTION PERFORMANCE IN COMPARISON WITH SOTA TRAJECTORY PREDICTION MODELS. THE RESULTS ARE PRESENTED IN MINADE₆/MINFDE₆.

| | All | Top 10% | Top 5% |
|----------------|------------------|------------------|------------------|
| VectorNet [26] | 1.11/2.90 | 2.06/3.61 | 2.65/4.60 |
| LaneGCN [25] | 1.07/1.84 | 1.99/3.50 | 2.55/4.47 |
| MTR [20] | 0.86/1.57 | 1.64/3.05 | 2.00/3.89 |
| QCNet [21] | 0.78/1.41 | 1.45/2.77 | 1.77/3.55 |
| CDKFormer | 0.75/1.42 | 1.33/2.58 | 1.44/2.92 |

3) *Metrics*: We adopt the commonly used trajectory prediction metric: minimum average displacement error (minADE_k) and minimum final displacement error (minFDE_k) between K trajectory samples and the ground truth to measure the accuracy of trajectory prediction, as calculated below:

$$\text{minADE}_k = \frac{1}{t_f} \min_k \sum_{t=1}^{t_f} \|\hat{y}_k^t - y^t\|^2 \quad (27)$$

$$\text{minFDE}_k = \min_k \|\hat{y}_k^{t_f} - y^{t_f}\|^2 \quad (28)$$

where \hat{y}_k^t denotes the k -th predicted future position of the target vehicle at time t , and y^t denotes the ground truth future position at time t .

We further evaluate our model’s performance on both head and tail samples to validate its effectiveness in long-tailed scenarios. Specifically, we report the minADE_k and minFDE_k scores for the top 5% and 10% tailed samples, which are selected based on the long-tail score S .

4) *Implementation Details*: The model is trained on a server with 4 NVIDIA GeForce RTX 4090 GPUs. We set the embedding dimension to 64. The tail weight α is 0.1. The number of encoder and decoder layers is set to 2. The training is conducted for 30 epochs. The Adam optimizer is used with an initial learning rate of 0.003 and a weight decay rate of 0.01. A cosine learning rate scheduler is employed to adjust the learning rate during training. The batch size is set to 16. The implementation is based on Python 3.9 and PyTorch 2.0.

B. Overall Performance

We first compare the performance of our model with SOTA models on Argoverse 2 motion forecasting dataset (validation set). The results are presented in Table II.

CDKFormer achieves a minADE₆ of 0.75 m and a minFDE₆ of 1.42 m on all samples, achieving comparable performance to SOTA models. Compared to a recent strong baseline QCNet [21], the proposed model achieves a 2.56% reduction in minADE₆. And a 9.55% reduction in minFDE₆ compared to MTR [20] is observed. Compared to earlier graph-based models, our model demonstrates significant performance improvements. For example, when compared to LaneGCN [25], CDKFormer achieves 22.83% lower minFDE₆, which can be attributed to the design of our attention-based feature fusion technique and query-based decoding paradigm.

TABLE III
PREDICTION PERFORMANCE IN COMPARISON WITH SOTA LONG-TAIL
LEARNING METHODS. THE RESULTS ARE PRESENTED IN
MINADE₆/MINFDE₆.

| | All | Top 10% | Top 5% |
|---------------------------|-------------------|------------------|------------------|
| QCNet [21] | 0.78/ 1.41 | 1.45/2.77 | 1.77/3.55 |
| QCNet + Balanced Sampling | 0.80/1.45 | 1.45/2.74 | 1.74/3.48 |
| QCNet + Loss reweighting | 0.79/1.44 | 1.45/2.75 | 1.76/3.50 |
| QCNet + Contrastive [13] | 0.78/1.43 | 1.44/2.74 | 1.75/3.49 |
| QCNet + FEND [14] | 0.77/1.43 | 1.43/2.73 | 1.73/3.46 |
| CDKFormer | 0.75/1.42 | 1.33/2.58 | 1.44/2.92 |

TABLE IV
ABLATION STUDY ON INPUT DEVIATION FEATURE. THE RESULTS ARE
PRESENTED IN MINADE₆/MINFDE₆.

| Individual | Group | All | Top 10% | Top 5% |
|------------|-------|------------------|------------------|------------------|
| | | 0.78/1.46 | 1.38/2.71 | 1.50/3.10 |
| ✓ | | 0.75/1.44 | 1.35/2.62 | 1.47/2.97 |
| | ✓ | 0.77/1.45 | 1.37/2.65 | 1.49/3.01 |
| ✓ | ✓ | 0.75/1.42 | 1.33/2.58 | 1.44/2.92 |

C. Long-Tail Performance

The long-tail performance of CDKFormer is promising compared to SOTA trajectory prediction models, including long-tail prediction methods. As shown in Table II, our model demonstrates significant improvements on the top 10% and top 5% tailed samples, achieving a minFDE₆ of 2.58 m and 2.92 m, respectively, outperforming QCNet and other recent models in both metrics by a large margin.

Furthermore, our model exhibits considerable improvements over existing SOTA long-tail learning methods. As illustrated in Table III, traditional imbalanced learning methods show suboptimal performance. Specifically, balanced sampling results in a minADE₆ of 1.74 m on top% samples, while loss reweighting achieves a minADE₆ of 1.45 m on top 5% samples. Contrastive learning-based methods, such as Contrastive [13] and FEND [14], exhibit limited improvements in long-tail performance. For instance, contrastive learning achieves a minADE₆ of 1.44 m and a minFDE₆ of 2.74 m on top 10% samples. For the top 5% tailed samples, the proposed CDKFormer achieves a 15.61% improvement on minFDE₆, significantly surpassing FEND by a large margin.

D. Ablation Study

1) *Ablation Study on Input Deviation Feature:* As shown in Table IV, the results of the ablation study indicate that incorporating both individual deviation and group deviation features significantly enhances the model performance, particularly in challenging scenarios. A baseline model with no deviation feature reaches a minADE₆ of 0.78 m, 1.38 m and 1.50 m on all, top 10% and top 5% samples, respectively. When only individual deviation is included, the model demonstrates certain improvements. On the top 10% tailed samples, where the minADE₆ is reduced to 1.35 m from 1.38 m, and the minFDE₆ is 2.62 m. Similarly, including only group deviation also leads to moderate performance gains. The best overall performance

TABLE V
ABLATION STUDY ON QUERY DESIGN. THE RESULTS ARE PRESENTED IN
MINADE₆/MINFDE₆.

| | | Query | | All | Top 10% | Top 5% |
|------|------|--------|-------------|-------------------|------------------|------------------|
| Mode | (R.) | Future | (T.) Future | | | |
| ✓ | | | | 0.79/1.52 | 1.40/2.76 | 1.51/3.11 |
| | | ✓ | | 0.91/1.48 | 1.50/2.75 | 1.62/3.19 |
| ✓ | | ✓ | | 0.76/ 1.42 | 1.34/2.60 | 1.45/2.94 |
| ✓ | | | ✓ | 0.77/1.46 | 1.36/2.66 | 1.48/3.03 |
| ✓ | | ✓ | ✓ | 0.75/1.42 | 1.33/2.58 | 1.44/2.92 |

is achieved when both individual deviation and group deviation are used together. The model achieves a minADE₆ of 0.75 m and a minFDE₆ of 1.42 m. On tailed samples, we also observe a notable improvement over the baseline model, with a 3.62% and 4.00% reduction of minADE₆ across the top 10% and 5% samples. This highlights the importance of integrating both individual and group deviation features to improve long-tail trajectory prediction.

2) *Ablation Study on Query Design:* In this ablation study, we evaluate the effect of different decoding queries on the performance of the CDKFormer decoder, as shown in Table V. The loss of one query is abandoned if the corresponding query is removed. The deviation feature is always retained in the decoder.

The results indicate that using only the mode query or the regular future query leads to a performance drop, particularly on the tailed samples. A marked improvement is observed when the mode query and regular future query are combined, yielding a minFDE₆ of 1.42 m and 2.60 m on all samples and top 10% samples, respectively. Pairing the mode query with the tail future query achieves a minADE₆ of 0.77 m and 1.48 m on all samples and top 5% samples. However, this configuration performs slightly worse than the mode and regular future query combination. The optimal performance is attained when all three queries are utilized together. A 0.77% and 0.68% reduction in minFDE₆ on top 10% and top 5% samples are observed, compared to the model with only the mode and regular future query. These findings highlight the importance of incorporating dual queries to effectively capture temporal patterns and enhance robustness in long-tail trajectory prediction scenarios.

3) *Ablation Study on Multistream Cross-Attention Block Structure:* As illustrated in Table VI, the results of the ablation study on the multistream cross-attention block structure highlight the effect of different stream sequences and the number of layers on prediction performance. Overall, the results suggest that the sequence Deviation→Context→Self offers the best performance in terms of both minADE₆ and minFDE₆ on difference sets. It achieves a marginal improvement of 1.32%, 2.21% and 2.04% in minADE₆ compared to the sequence Context→Deviation→Self on all, top 10% and top 5% data, respectively, probably due to the fusion of deviation feature in the first place. The traditional Transformer Decoder-like self-attention→cross-attention scheme does not get the best result, highlighting the importance of the specific order in which the

TABLE VI
ABLATION STUDY ON MULTISTREAM CROSS-ATTENTION BLOCK STRUCTURE

| Stream sequence | #Layers | All | | Top 10% | | Top 5% | |
|------------------------|---------|-------------------------|-------------------------|-------------------------|-------------------------|-------------------------|-------------------------|
| | | minADE ₆ (m) | minFDE ₆ (m) | minADE ₆ (m) | minFDE ₆ (m) | minADE ₆ (m) | minFDE ₆ (m) |
| Self→Deviation→Context | 2 | 0.77 | 1.44 | 1.36 | 2.64 | 1.47 | 2.99 |
| Context→Deviation→Self | 2 | 0.76 | 1.45 | 1.36 | 2.67 | 1.47 | 3.05 |
| Deviation→Context→Self | 1 | 0.82 | 1.53 | 1.43 | 2.71 | 1.61 | 3.17 |
| Deviation→Context→Self | 2 | 0.75 | 1.42 | 1.33 | 2.58 | 1.44 | 2.92 |
| Deviation→Context→Self | 3 | 0.75 | 1.40 | 1.32 | 2.57 | 1.43 | 2.90 |

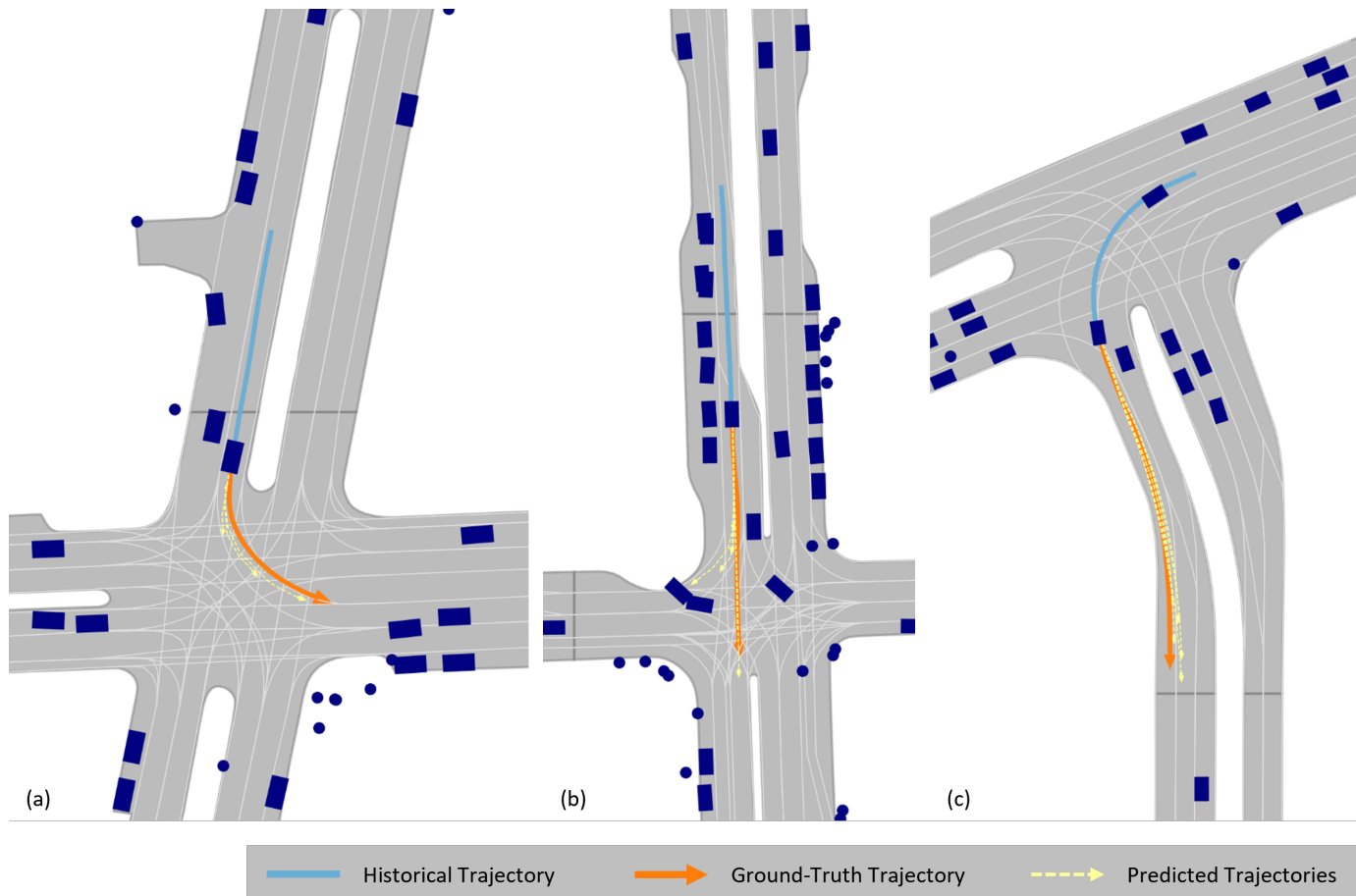


Fig. 8. Visualization of CDKFormer multimodal trajectory prediction results. Vehicles are represented by bounding boxes in dark blue. Historical and ground-truth trajectories are illustrated with light blue and orange solid lines, respectively. The predicted multimodal future trajectories are shown by yellow dash lines.

streams are processed.

Increasing the number of layers yields a notable enhancement in model performance. Specifically, the two-layer model yielding a minFDE₆ of 1.42 m across all samples, achieving a 7.19% improvement compared to the one-layer model. The three-layer model achieves a minADE₆ of 0.75 m and a minFDE₆ of 1.40 m, showing minimal gains compared to the two-layer model, which suggests that further increases in depth may yield diminishing returns or require additional optimization to fully realize their potential.

E. Qualitative Analysis

To evaluate the reliability of the proposed model, particularly in challenging conditions, we present visualizations of

the trajectory prediction results in three representative long-tail scenarios. Fig. 8(a) depicts the target vehicle executing a left turn at an intersection. The model’s multimodal predictions accurately align with the lane segments and capture the left turn maneuver, accounting for various possible speeds. Fig. 8(b) presents a more complex scenario in which the target vehicle proceeds straight through the intersection. The proposed CDKFormer successfully predicts the trajectory required to go straight and also generates alternative trajectories for a possible right turn, demonstrating its ability to handle multiple potential behaviors. Fig. 8(c) illustrates a scenario involving a long-range trajectory where the target vehicle executes a left turn, with the intention of the target vehicle already shown from its historical trajectory. CDKFormer accurately predicts

the future path, showcasing its effectiveness in leveraging past motion and deviation information for accurate forecasting.

VI. CONCLUSIONS

In this study, we introduce CDKFormer, a novel framework tailored for long-tail trajectory prediction. Our approach addresses the challenges posed by long-tailed distributions in trajectory prediction tasks, ensuring robust performance across diverse scenarios. This study begins with a comprehensive analysis of long-tail characteristics of a large-scale trajectory prediction dataset, from which we derive features that effectively characterize long-tailed samples. Leveraging the extracted features, we propose the Contextual Deviation Knowledge-based Transformer (CDKFormer) model. We design a scene context encoding module and a deviation feature fusion module composed of Transformer encoder layers to integrate scene contextual information and obtain a comprehensive representation of the driving environment. Subsequently, a dual query-based decoder is developed. Employing a multistream decoder block, we leverage a mode query and dual future queries to decode heterogeneous scene deviation features. The dual queries, including regular and tail future queries, are specifically designed to encapsulate both normal-state and tail-state information. These queries are then integrated into the standard scene query, enabling subsequent refinement and multimodal trajectory generation.

We evaluate the proposed model using the Argoverse 2 Motion Forecasting dataset, where CDKFormer achieves SOTA performance across multiple evaluation metrics, confirming its effectiveness in predicting future trajectories under long-tailed conditions. Ablation studies further substantiate the contributions of each component, highlighting their individual and collective impact on overall performance. Collectively, our method provides a robust framework for understanding long-tailed scenarios and introduces a new perspective on trajectory prediction models in rare and challenging scenarios.

One possible direction for future research is to expand deviation modeling to account for multiple interacting agents within complex traffic environments. While the present study primarily centers on deviation modeling for the target vehicle, exploring the relationship between the deviation states of surrounding agents and subsequently using it for multiagent prediction could significantly improve the model performance in real-world settings. Another promising direction is to account for heterogeneity among surrounding agents. While the current CDKFormer can handle a variety of traffic agents as the inputs, explicitly considering the types of surrounding agents and modeling their heterogeneity in long-tail trajectory prediction could significantly enhance the model's performance. This approach would better capture the diverse behaviors of pedestrians, cyclists, vehicles, etc., potentially benefiting the robustness of autonomous systems in complex and real-world scenarios.

REFERENCES

- [1] Y. Huang, J. Du, Z. Yang, Z. Zhou, L. Zhang, and H. Chen, "A survey on trajectory-prediction methods for autonomous driving," *IEEE Transactions on Intelligent Vehicles*, vol. 7, no. 3, pp. 652–674, 2022.
- [2] Q. Wang, D. Xu, G. Kuang, C. Lv, S. E. Li, and B. Nie, "Risk-aware vehicle trajectory prediction under safety-critical scenarios," *IEEE Transactions on Intelligent Transportation Systems*, 2025.
- [3] K. Yang, S. Li, Y. Chen, D. Cao, and X. Tang, "Towards safe decision-making for autonomous vehicles at unsignalized intersections," *IEEE Transactions on Vehicular Technology*, 2024.
- [4] Q. Liu, K. Zhang, M. Li, X. Chen, X. Lin, and S. Li, "Integrated optimization of traffic signal timings and vehicle trajectories considering mandatory lane-changing at isolated intersections," *Transportation Research Part C: Emerging Technologies*, vol. 163, p. 104614, 2024.
- [5] S. Ettinger, S. Cheng, B. Caine, C. Liu, H. Zhao, S. Pradhan, Y. Chai, B. Sapp, C. R. Qi, Y. Zhou *et al.*, "Large scale interactive motion forecasting for autonomous driving: The waymo open motion dataset," in *Proceedings of the IEEE/CVF International Conference on Computer Vision*, 2021, pp. 9710–9719.
- [6] B. Wilson, W. Qi, T. Agarwal, J. Lambert, J. Singh, S. Khandelwal, B. Pan, R. Kumar, A. Hartnett, J. K. Pontes *et al.*, "Argoverse 2: Next generation datasets for self-driving perception and forecasting," *arXiv preprint arXiv:2301.00493*, 2023.
- [7] H. Caesar, V. Bankiti, A. H. Lang, S. Vora, V. E. Liong, Q. Xu, A. Krishnan, Y. Pan, G. Baldan, and O. Beijbom, "nuscenes: A multi-modal dataset for autonomous driving," in *Proceedings of the IEEE/CVF conference on Computer Vision and Pattern Recognition*, 2020, pp. 11 621–11 631.
- [8] H. X. Liu and S. Feng, "Curse of rarity for autonomous vehicles," *Nature Communications*, vol. 15, no. 1, p. 4808, 2024.
- [9] W. Ding, C. Xu, M. Arief, H. Lin, B. Li, and D. Zhao, "A survey on safety-critical driving scenario generation—a methodological perspective," *IEEE Transactions on Intelligent Transportation Systems*, 2023.
- [10] M. Bahari, S. Saadatnejad, A. Rahimi, M. Shaverdikondori, A. H. Shahidzadeh, S.-M. Moosavi-Dezfooli, and A. Alahi, "Vehicle trajectory prediction works, but not everywhere," in *Proceedings of the IEEE/CVF Conference on Computer Vision and Pattern Recognition*, 2022, pp. 17 123–17 133.
- [11] Y. Li, S. Z. Zhao, C. Xu, C. Tang, C. Li, M. Ding, M. Tomizuka, and W. Zhan, "Pre-training on synthetic driving data for trajectory prediction," in *2024 IEEE/RSJ International Conference on Intelligent Robots and Systems (IROS)*. IEEE, 2024, pp. 5910–5917.
- [12] J. Kozerawski, M. Sharan, and R. Yu, "Taming the long tail of deep probabilistic forecasting," *arXiv preprint arXiv:2202.13418*, 2022.
- [13] O. Makansi, Ö. Cicek, Y. Marrakchi, and T. Brox, "On exposing the challenging long tail in future prediction of traffic actors," in *Proceedings of the IEEE/CVF International Conference on Computer Vision*, 2021, pp. 13 147–13 157.
- [14] Y. Wang, P. Zhang, L. Bai, and J. Xue, "Fend: A future enhanced distribution-aware contrastive learning framework for long-tail trajectory prediction," in *Proceedings of the IEEE/CVF Conference on Computer Vision and Pattern Recognition*, 2023, pp. 1400–1409.
- [15] R. C. Mercurius, E. Ahmadi, S. M. A. Shabestary, and A. Rasouli, "Amend: A mixture of experts framework for long-tailed trajectory prediction," *arXiv preprint arXiv:2402.08698*, 2024.
- [16] C.-F. Lin, A. G. Ulsoy, and D. J. LeBlanc, "Vehicle dynamics and external disturbance estimation for vehicle path prediction," *IEEE Transactions on Control Systems Technology*, vol. 8, no. 3, pp. 508–518, 2000.
- [17] A. Polychronopoulos, M. Tsogas, A. J. Amditis, and L. Andreone, "Sensor fusion for predicting vehicles' path for collision avoidance systems," *IEEE Transactions on Intelligent Transportation Systems*, vol. 8, no. 3, pp. 549–562, 2007.
- [18] T. Gindele, S. Brechtel, and R. Dillmann, "A probabilistic model for estimating driver behaviors and vehicle trajectories in traffic environments," in *13th International IEEE Conference on Intelligent Transportation Systems*. IEEE, 2010, pp. 1625–1631.
- [19] T. Salzmann, B. Ivanovic, P. Chakravarty, and M. Pavone, "Trajectron++: Dynamically-feasible trajectory forecasting with heterogeneous data," in *Computer Vision—ECCV 2020: 16th European Conference, Glasgow, UK, August 23–28, 2020, Proceedings, Part XVIII 16*. Springer, 2020, pp. 683–700.
- [20] S. Shi, L. Jiang, D. Dai, and B. Schiele, "Motion transformer with global intention localization and local movement refinement," *Advances in Neural Information Processing Systems*, vol. 35, pp. 6531–6543, 2022.
- [21] Z. Zhou, J. Wang, Y.-H. Li, and Y.-K. Huang, "Query-centric trajectory prediction," in *Proceedings of the IEEE/CVF Conference on Computer Vision and Pattern Recognition*, 2023, pp. 17 863–17 873.
- [22] M. Geng, J. Li, Y. Xia, and X. M. Chen, "A physics-informed transformer model for vehicle trajectory prediction on highways," *Transportation Research Part C: Emerging Technologies*, vol. 154, p. 104272, 2023.

- [23] Z. Zhang, C. Wang, W. Zhao, M. Cao, and J. Liu, "Ego vehicle trajectory prediction based on time-feature encoding and physics-intention decoding," *IEEE Transactions on Intelligent Transportation Systems*, 2024.
- [24] K. Yang, S. Li, M. Wang, and X. Tang, "Interactive decision-making integrating graph neural networks and model predictive control for autonomous driving," *IEEE Transactions on Intelligent Transportation Systems*, 2025.
- [25] M. Liang, B. Yang, R. Hu, Y. Chen, R. Liao, S. Feng, and R. Urtasun, "Learning lane graph representations for motion forecasting," in *Computer Vision—ECCV 2020: 16th European Conference, Glasgow, UK, August 23–28, 2020, Proceedings, Part II 16*. Springer, 2020, pp. 541–556.
- [26] J. Gao, C. Sun, H. Zhao, Y. Shen, D. Anguelov, C. Li, and C. Schmid, "Vectornet: Encoding hd maps and agent dynamics from vectorized representation," in *Proceedings of the IEEE/CVF conference on Computer Vision and Pattern Recognition*, 2020, pp. 11 525–11 533.
- [27] X. Mo, H. Liu, Z. Huang, X. Li, and C. Lv, "Map-adaptive multimodal trajectory prediction via intention-aware unimodal trajectory predictors," *IEEE Transactions on Intelligent Transportation Systems*, 2023.
- [28] Y. Liu, J. Zhang, L. Fang, Q. Jiang, and B. Zhou, "Multimodal motion prediction with stacked transformers," in *Proceedings of the IEEE/CVF conference on Computer Vision and Pattern Recognition*, 2021, pp. 7577–7586.
- [29] C. Yu, X. Ma, J. Ren, H. Zhao, and S. Yi, "Spatio-temporal graph transformer networks for pedestrian trajectory prediction," in *Computer Vision—ECCV 2020: 16th European Conference, Glasgow, UK, August 23–28, 2020, Proceedings, Part XII 16*. Springer, 2020, pp. 507–523.
- [30] Y. Lian, K. Zhang, M. Li, and J. Lin, "Hierarchical transformer-based red-light running prediction model for two-wheelers with multitask learning," *IEEE Transactions on Intelligent Vehicles*, 2024.
- [31] Y. Yuan, X. Weng, Y. Ou, and K. M. Kitani, "Agentformer: Agent-aware transformers for socio-temporal multi-agent forecasting," in *Proceedings of the IEEE/CVF International Conference on Computer Vision*, 2021, pp. 9813–9823.
- [32] N. Carion, F. Massa, G. Synnaeve, N. Usunier, A. Kirillov, and S. Zagoruyko, "End-to-end object detection with transformers," in *European Conference on Computer Vision*. Springer, 2020, pp. 213–229.
- [33] Z. Lan, Y. Jiang, Y. Mu, C. Chen, and S. E. Li, "Sept: Towards efficient scene representation learning for motion prediction," in *The Twelfth International Conference on Learning Representations*, 2023.
- [34] J. Gu, C. Sun, and H. Zhao, "Densent: End-to-end trajectory prediction from dense goal sets," in *Proceedings of the IEEE/CVF International Conference on Computer Vision*, 2021, pp. 15 303–15 312.
- [35] H. Zhao, J. Gao, T. Lan, C. Sun, B. Sapp, B. Varadarajan, Y. Shen, Y. Shen, Y. Chai, C. Schmid *et al.*, "Tnt: Target-driven trajectory prediction," in *Conference on Robot Learning*. PMLR, 2021, pp. 895–904.
- [36] B. Zhang, N. Song, and L. Zhang, "Decoupling motion forecasting into directional intentions and dynamic states," *Advances in Neural Information Processing Systems*, vol. 37, pp. 106 582–106 606, 2025.
- [37] J. Li, J. Li, S. Bae, and D. Isele, "Adaptive prediction ensemble: Improving out-of-distribution generalization of motion forecasting," *IEEE Robotics and Automation Letters*, 2024.
- [38] Q. Zhang, S. Hu, J. Sun, Q. A. Chen, and Z. M. Mao, "On adversarial robustness of trajectory prediction for autonomous vehicles," in *Proceedings of the IEEE/CVF Conference on Computer Vision and Pattern Recognition*, 2022, pp. 15 159–15 168.
- [39] J. Zhang, M. Pourkeshavarz, and A. Rasouli, "Tract: A training dynamics aware contrastive learning framework for long-tail trajectory prediction," in *2024 IEEE Intelligent Vehicles Symposium (IV)*. IEEE, 2024, pp. 3282–3288.
- [40] B. Yang, K. Yan, C. Hu, H. Hu, Z. Yu, and R. Ni, "Dynamic subclass-balancing contrastive learning for long-tail pedestrian trajectory prediction with progressive refinement," *IEEE Transactions on Automation Science and Engineering*, 2024.
- [41] Z. Lan, Y. Ren, H. Yu, L. Liu, Z. Li, Y. Wang, and Z. Cui, "Hi-scl: Fighting long-tailed challenges in trajectory prediction with hierarchical wave-semantic contrastive learning," *Transportation Research Part C: Emerging Technologies*, vol. 165, p. 104735, 2024.
- [42] Y. Zhou, H. Shao, L. Wang, S. L. Waslander, H. Li, and Y. Liu, "Smart-pretrain: Model-agnostic and dataset-agnostic representation learning for motion prediction," *arXiv preprint arXiv:2410.08669*, 2024.
- [43] Y. Zhang, B. Kang, B. Hooi, S. Yan, and J. Feng, "Deep long-tailed learning: A survey," *IEEE Transactions on Pattern Analysis and Machine Intelligence*, 2023.
- [44] Y. Yang, K. Zha, Y. Chen, H. Wang, and D. Katabi, "Delving into deep imbalanced regression," in *International conference on machine learning*. PMLR, 2021, pp. 11 842–11 851.
- [45] O. Makansi, O. Cicek, K. Buchicchio, and T. Brox, "Multimodal future localization and emergence prediction for objects in egocentric view with a reachability prior," in *Proceedings of the IEEE/CVF Conference on Computer Vision and Pattern Recognition*, 2020, pp. 4354–4363.
- [46] M. Tancik, P. Srinivasan, B. Mildenhall, S. Fridovich-Keil, N. Raghavan, U. Singhal, R. Ramamoorthi, J. Barron, and R. Ng, "Fourier features let networks learn high frequency functions in low dimensional domains," *Advances in Neural Information Processing Systems*, vol. 33, pp. 7537–7547, 2020.
- [47] C. R. Qi, H. Su, K. Mo, and L. J. Guibas, "Pointnet: Deep learning on point sets for 3d classification and segmentation," in *Proceedings of the IEEE Conference on Computer Vision and Pattern Recognition*, 2017, pp. 652–660.
- [48] J. Cheng, X. Mei, and M. Liu, "Forecast-mae: Self-supervised pre-training for motion forecasting with masked autoencoders," in *Proceedings of the IEEE/CVF International Conference on Computer Vision*, 2023, pp. 8679–8689.